

Genome-wide probing of RNA structure reveals active unfolding of mRNA structures *in vivo*

Silvi Rouskin¹, Meghan Zubradt¹, Stefan Washietl^{2,3,4}, Manolis Kellis^{2,3,4} & Jonathan S. Weissman¹

RNA has a dual role as an informational molecule and a direct effector of biological tasks. The latter function is enabled by RNA's ability to adopt complex secondary and tertiary folds and thus has motivated extensive computational^{1,2} and experimental^{3–8} efforts for determining RNA structures. Existing approaches for evaluating RNA structure have been largely limited to *in vitro* systems, yet the thermodynamic forces which drive RNA folding *in vitro* may not be sufficient to predict stable RNA structures *in vivo*⁵. Indeed, the presence of RNA-binding proteins and ATP-dependent helicases can influence which structures are present inside cells. Here we present an approach for globally monitoring RNA structure in native conditions *in vivo* with single-nucleotide precision. This method is based on *in vivo* modification with dimethyl sulphate (DMS), which reacts with unpaired adenine and cytosine residues⁹, followed by deep sequencing to monitor modifications. Our data from yeast and mammalian cells are in excellent agreement with known messenger RNA structures and with the high-resolution crystal structure of the *Saccharomyces cerevisiae* ribosome¹⁰. Comparison between *in vivo* and *in vitro* data reveals that in rapidly dividing cells there are vastly fewer structured mRNA regions *in vivo* than *in vitro*. Even thermo-stable RNA structures are often denatured in cells, highlighting the importance of cellular processes in regulating RNA structure. Indeed, analysis of mRNA structure under ATP-depleted conditions in yeast shows that energy-dependent processes strongly contribute to the predominantly unfolded state of mRNAs inside cells. Our studies broadly enable the functional analysis of physiological RNA structures and reveal that, in contrast to the Anfinsen view of protein

folding whereby the structure formed is the most thermodynamically favourable, thermodynamics have an incomplete role in determining mRNA structure *in vivo*.

A wide range of chemicals and enzymes have been used to monitor RNA structure^{7,11}. We focused on DMS as it enters cells rapidly^{9,12} and is a well-established tool for the analysis of RNA structure¹³. DMS is highly reactive with solvent-accessible, unpaired residues but reliably unreactive with bases engaged in Watson–Crick interactions, thus nucleotides that are strongly protected or reactive to DMS can be inferred to be base-paired or unpaired, respectively. We coupled DMS treatment to a massively parallel sequencing readout (DMS-seq) by randomly fragmenting the pool of modified RNAs and size-selecting before 3' ligation with a specific adaptor oligonucleotide (Fig. 1a). Because DMS modifications at adenine and cytosine residues block reverse transcription¹⁴, we used a second size-selection step to collect and sequence only the prematurely terminated complementary DNA fragments. Sequencing of the fragments reveals the precise site of DMS modification, with the number of reads at each position providing a measure of relative reactivity of that site. The results are highly reproducible and robust against changes in the time of modification or concentration of DMS used (Fig. 1b). The sequencing readout allowed global analysis with a high signal-to-noise ratio—in DMS treated samples, >90% of reads end with an adenine and cytosine, corresponding to false positives for A and C of 7% and 17%, respectively (Fig. 1c). For each experiment, we measured RNA structure both *in vivo* and *in vitro* (that is, refolded RNA in the absence of proteins). We also measured DMS reactivity under denaturing conditions (95 °C) as a control for intrinsic biases in reactivity, library

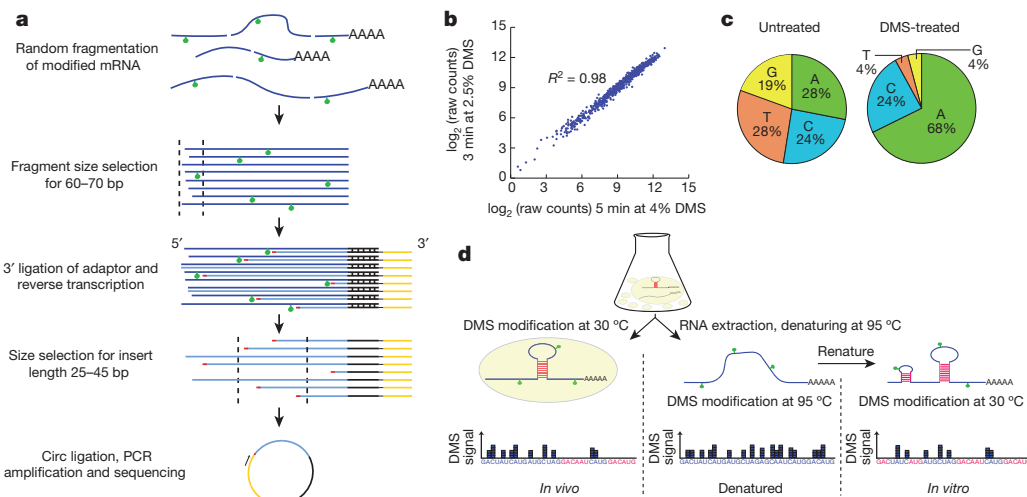


Figure 1 | Using dimethyl sulphate for RNA structure probing by deep sequencing. **a**, Schematic of strategy for library preparation with DMS-modified RNAs. **b**, DMS-seq data are highly reproducible between biological replicates and robust against changes in time and DMS concentration. **c**, *In vivo*

DMS treatment markedly enriches for sequencing reads mapping to A/C bases compared to untreated control. **d**, DMS-seq was completed for *in vivo*, denatured and *in vitro* samples. The denatured sample served as an ‘unstructured’ control.

¹Department of Cellular and Molecular Pharmacology, California Institute of Quantitative Biology, Center for RNA Systems Biology, Howard Hughes Medical Institute, University of California, San Francisco, California 94158, USA. ²Department of Electrical Engineering and Computer Science, Massachusetts Institute of Technology, Cambridge, Massachusetts 02139, USA. ³Computer Science and Artificial Intelligence Laboratory, Massachusetts Institute of Technology, Cambridge, Massachusetts 02139, USA. ⁴The Broad Institute, Cambridge, Massachusetts 02139, USA.

generation or sequencing, revealing only modest variability compared to that caused by structure-dependent differences in reactivity (Fig. 2c and Extended Data Fig. 1a).

The *in vivo* DMS-seq data are in excellent agreement with known RNA structures. We examined three validated mRNA structures in *S. cerevisiae*: *HAC1*, *RPS28B* and *ASH1*^{15–18}. In each case, the DMS-seq pattern qualitatively recapitulates secondary structure with high reactivity constrained to loop regions in both the *in vivo* and the *in vitro* samples, but not in the denatured samples (Fig. 2a, b). Recent determination of a high-resolution yeast 80S ribosome crystal structure¹⁰ allowed us to comprehensively evaluate the DMS-seq data for ribosomal RNAs. Comparison of the 18S (Fig. 2c) and 25S (Extended Data Fig. 1b) rRNA DMS signal *in vivo* versus denatured reveals a large number of strongly protected bases *in vivo*. Based on DMS reactivity, we used a threshold to bin bases into reactive and unreactive groups, then calculated agreement with the crystal structure model as a function of the threshold. True positives were defined as both unpaired and solvent-accessible bases according to the crystal structure, and true negatives defined as paired bases. A receiver operator characteristic (ROC) curve shows a range of thresholds with superb agreement between the *in vivo* DMS-seq data and the crystal structure model (Fig. 2d). For example, at a threshold of 0.2, the true positive rate, false positive rate and accuracy are 90%, 6% and 94%, respectively. Bases that were not reactive at this threshold *in vivo* showed normal reactivity when denatured (Extended Data Fig. 1c). This indicates that the small fraction (~10%) of residues that are designated as accessible, but are nonetheless strongly protected from reacting with DMS, resulted from genuine

differences in the *in vivo* conformation of the ribosome and the existing crystal structures. Agreement with the crystal structure was far less good for *in vitro* refolded rRNA (as expected given the absence of ribosomal proteins) and was completely absent for denatured RNA. By contrast, probing of intact purified ribosomes gave a very similar result to that seen *in vivo*, further demonstrating that DMS-seq yields comparable results *in vitro* and *in vivo* when probing the same structure.

Qualitatively, we observed many mRNA regions where structure was apparent *in vitro* but not *in vivo*. For example, computational analysis¹⁹ predicts a stem-loop structure in *RPL33A*. The *in vitro* DMS-seq data strongly supported this predicted structure, whereas this region showed little to no evidence of structure in cells (Fig. 3a). To explore systematically the relationship between mRNA structure *in vivo* and *in vitro*, we quantitated structure in a given region using two metrics: Pearson's correlation coefficient (*r* value), which reports on the degree of similarity of the modification pattern to that of a denatured control, and the Gini index²⁰, which measures disparity in count distribution as would be seen between an accessible loop versus a protected stem (Fig. 3b). We then applied these metrics to windows containing a total of 50 A/C nucleotides. Globally, mRNAs are much more structured *in vitro* compared to *in vivo*: there is a strong shift towards low *r* values and high Gini indices for the *in vitro* data that is far less pronounced *in vivo* (Fig. 3c). Thus unlike the rRNA, we find little evidence within mRNAs for *in vivo* DMS protection beyond what we observe *in vitro*, indicating that the DMS protection we observe *in vivo* is not due to mRNA–protein interactions. For example, using a cut-off (*r* value < 0.55, Gini index > 0.14) which captured the rRNAs and functionally validated mRNA

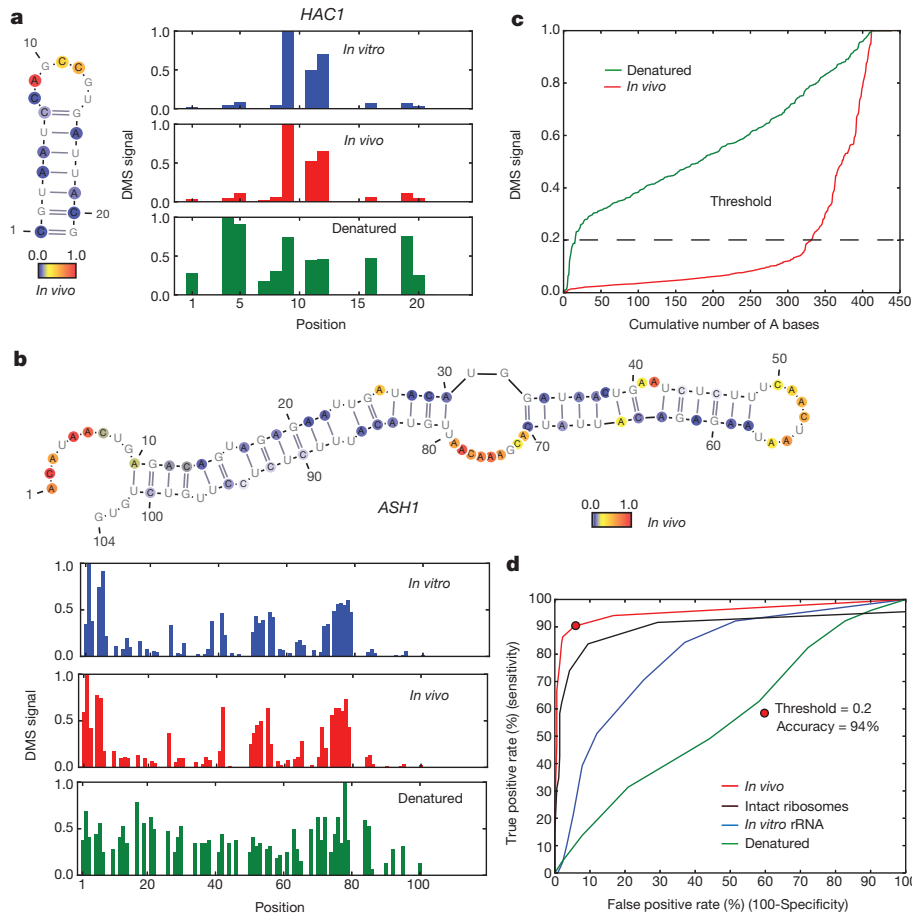


Figure 2 | Comparison of DMS-seq data to known RNA structures.

a, b, DMS signal in *HAC1* (position 1 corresponds to chromosome VI:75828) (a) and *ASH1* (position 1 corresponds to chromosome XI:96245) (b). Number of reads per position was normalized to the highest number of reads in the inspected region, which is set to 1.0. Also shown are the known secondary

structures with nucleotides colour-coded reflecting DMS-seq signal *in vivo*.

c, DMS signal on 18S rRNA A bases plotted from least to most reactive. d, ROC curve on the DMS signal for A/C bases from the 18S rRNA. Threshold at 94% accuracy corresponds to 0.2 for the A bases.

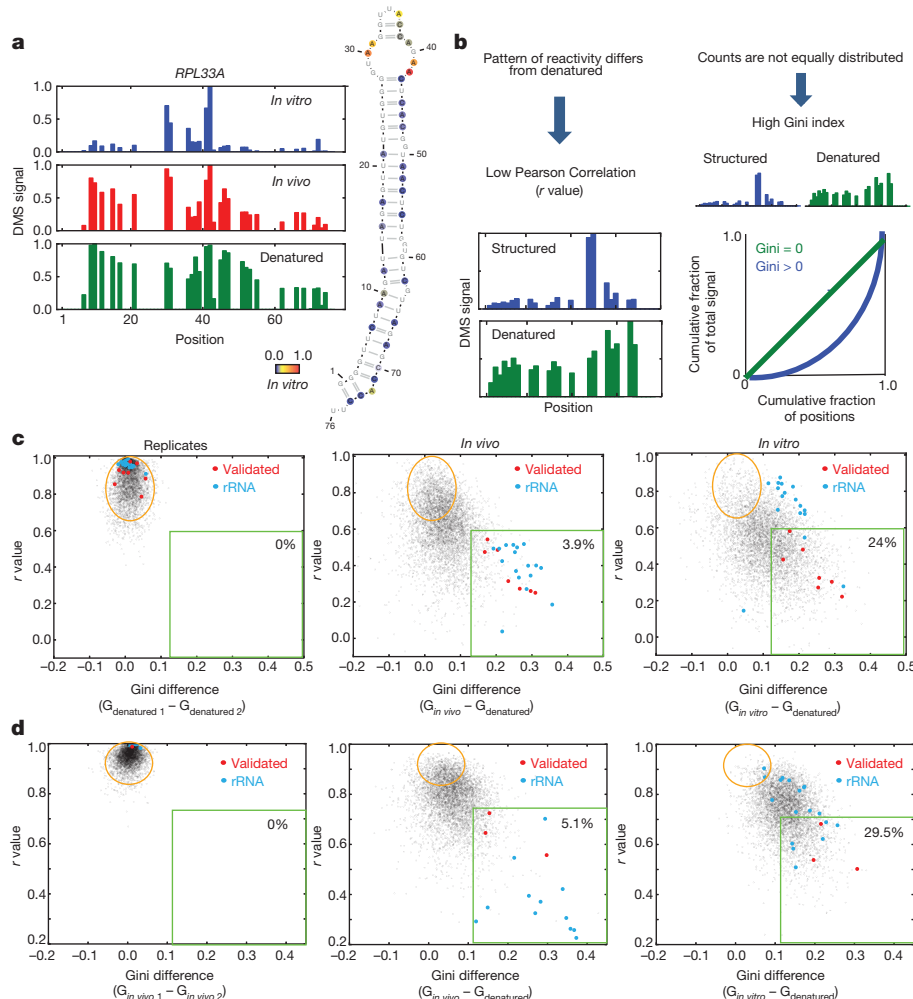


Figure 3 | Identification of structured mRNA regions reveals far less structure *in vivo* than *in vitro*. **a**, DMS signal in *RPL33A* mRNA, position 1 corresponds to chromosome XVI:282824. *In vitro* DMS signal colour-coded proportional to intensity and plotted onto the Mfold structure prediction. **b**, Schematic representation of the two metrics used to define structured regions within mRNAs. **c, d**, Scatter plots of Gini index difference versus *r* value from

biological replicates or *in vivo* and *in vitro* relative to denatured samples for non-overlapping mRNA regions of 50 A/C nucleotides of yeast (**c**) and K562 cells (**d**). A total of 5,000 randomly selected regions are shown. Red dots represent regions spanning validated mRNA structures and blue dots are regions from rRNA. Evaluated regions have a minimum of 15 reads per A/C on average and their total number for *in vivo* data are 23,412 (**c**) and 17,242 (**d**).

structures, including both previously characterized and newly identified structures (see below), we found that out of 23,412 mRNA regions examined (representing 1,948 transcripts), only 3.9% are structured *in vivo* compared to 24% *in vitro* (Fig. 3c and Extended Data Fig. 2 for similar results obtained with windows of different sizes). In addition, 29% of the regions *in vivo* are indistinguishable from denatured (Fig. 3c, orange circle), whereas *in vitro* only 9% of regions were fully denatured. We also applied DMS-seq to mammalian cells (both K562 cells and human foreskin fibroblasts), which revealed results qualitatively very similar to yeast—a limited number of stable structures *in vivo* compared to *in vitro* (Fig. 3d and Extended Data Figs 3 and 4).

Because the pool of stable structures seen *in vivo* includes previously validated functional mRNA structures, this relatively small subset of mRNA regions provides highly promising candidates for novel functional RNA structures. To explore this, we focused on two structured 5' untranslated regions (UTRs) from *PMA1* and *SFT2* and on the structured *PRC1* 3' UTR for more detailed functional analyses. We fused these UTRs upstream or downstream, respectively, of a Venus protein reporter and quantified Venus levels by flow cytometry. Stem loop structures in these UTRs significantly increased (5'SFT2) or decreased (5'PMA1 and 3'PRC1) protein levels upon disruption of their predicted base pairing interactions, and Venus protein levels were rescued by compensatory mutations (Extended Data Figs 5 and 6, Extended Data Table 1).

Phylogenetic analysis revealed the 5' UTR *PMA1* stem is under positive evolutionarily selection (Extended Data Fig. 5c), lending additional support for a physiological function. A list of 189 structured regions, along with a model of their secondary structures that are similarly supported by phylogenetic analysis of compensatory mutations, is hosted on an online database (<http://weissmanlab.ucsf.edu/yeaststructures/index.html>). In addition, we mutated predicted stems in three 3' UTRs with evidence of strongly ordered structures *in vitro* but not in cells, and these mutations resulted in minimal expression changes (Extended Data Fig. 6d). Nonetheless, it remains possible that transient, heterogeneous or weakly ordered structures *in vivo* have biological roles, especially if they become more ordered under different physiological conditions.

To evaluate what role *in vitro* thermodynamic stability has in driving mRNA folding *in vivo*, we performed genome-wide structure probing experiments *in vitro* at five temperatures (30, 45, 60, 75 and 95 °C). As temperature rises and structure unfolds (Fig. 4a), the DMS signal becomes more even (low Gini index) and the modification pattern resembles that of the 95 °C denatured control (high *r* value). We defined *in vitro* temperature of unfolding (T_{unfold}) as the lowest temperature where a region appeared similar to the denatured controls. Remarkably, many regions with little or no detectable structure *in vivo* show similar thermostability to highly structured regions, including structures that are functionally validated (Fig. 4a, b). For example, the regions of *RPL33A*

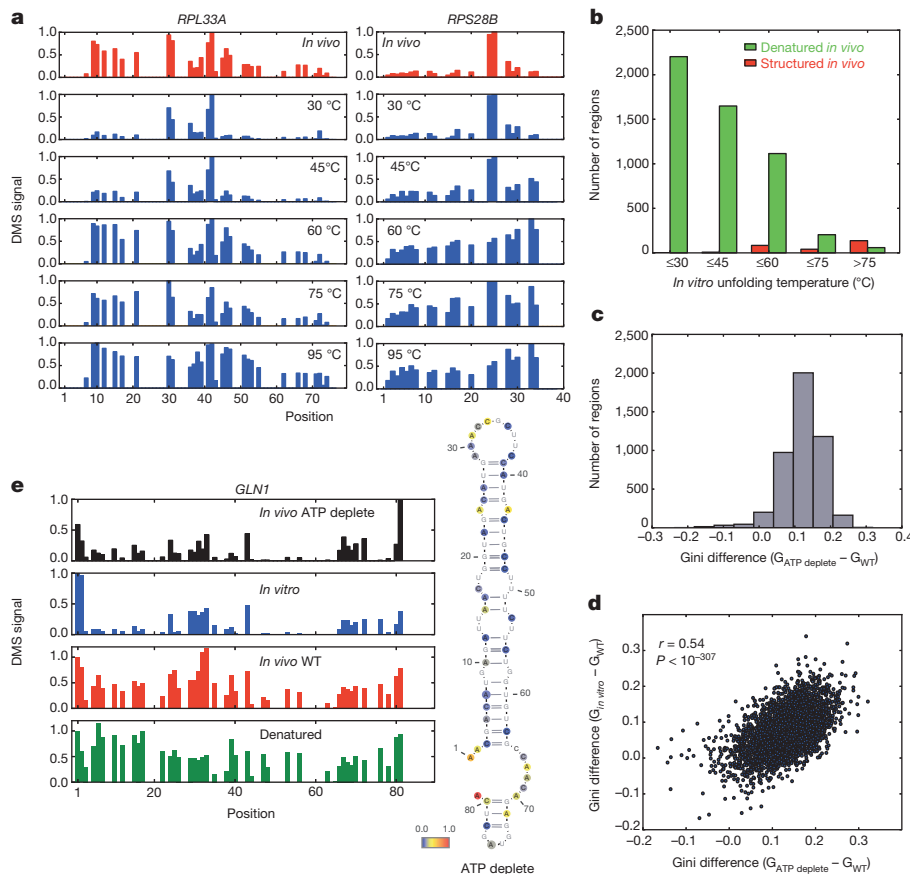


Figure 4 | Factors affecting the difference between mRNA structure *in vivo* and *in vitro*.

a, Example of DMS signal changes for *RPL33A* and *RPS28B* *in vivo* and *in vitro* with increasing temperature. **b**, Histogram of *in vitro* unfolding temperature (T_{unf}) for denatured (green bars) or structured (red bars) regions *in vivo*. **c**, Histogram of Gini index difference between ATP-depleted and wild-type yeast samples. **d**, Gini index differences in ATP-depleted yeast or *in vitro* refolded mRNAs relative to wild-type yeast, calculated over 50 A/C nucleotides. **e**, Example of *in vivo* structure changes during ATP depletion. Position 1 corresponds to chromosome XVI:643069.

(unfolded *in vivo*) and *RPS28B* (a functionally validated structure *in vivo*) are both highly structured *in vitro* and have $T_{unf} = 60$ °C. Nonetheless, we find that structures present *in vivo* do have a strong propensity for high thermostability (Fig. 4b), consistent with a recent *in vitro* mRNA thermal unfolding study⁸. In addition to the role of thermostability in explaining the disparity of RNA structure between *in vivo* and *in vitro* samples, we tested the effect of Mg²⁺ concentration *in vitro*. We obtained similar structure results with 2–6 mM Mg²⁺. However, at 1 mM Mg²⁺, we observe unfolding of most structures, including the functionally validated ones (Extended Data Fig. 7a). The above observations indicate that Mg²⁺ concentration and thermodynamic stability have an important but incomplete role in determining mRNA structure *in vivo*.

A central question is what accounts for the differences between *in vivo* and *in vitro* mRNA structure. Although translation by ribosomes has a role in unwinding structure, this is unlikely to be the dominant force for unfolding *in vivo* because the average *in vivo* structure for coding regions was not distinguishable from 5' and 3' UTRs (Extended Data Fig. 7b). Moreover, within coding regions, high ribosome occupancy of an mRNA as measured by ribosome profiling²¹ was not generally associated with lower structure (Extended Data Fig. 7c). It is likely that both active mechanisms (for example, RNA helicases) and passive mechanisms (for example, single-stranded-RNA binding proteins) counteract mRNA's intrinsic propensity to form the stable structures²² seen with *in vitro* studies^{3,23} and computational approaches¹⁹. To investigate how energy-dependent processes contribute to unfolding mRNA *in vivo*, we performed DMS-seq on yeast depleted of ATP²⁴. We observed a marked increase in mRNA structure *in vivo* following ATP depletion (Fig. 4c). Moreover, the structural changes seen upon ATP depletion are strongly correlated ($r = 0.54$, $P < 10^{-307}$) to the changes between *in vivo* and *in vitro* samples (Fig. 4d, e and Extended Data Fig. 8). We also observed a large increase in mRNA structure at 10 °C *in vivo* (Extended Data Fig. 9a), but these changes are not as strongly correlated with those seen upon ATP depletion (Extended Data Fig. 9b). Thus the mRNA

structures present in a cell are affected by a range of factors, underscoring the value of DMS-seq in defining the RNA structures present in a specific physiological condition or perturbation.

In summary, DMS-seq provides the first comprehensive exploration of RNA structure in a cellular environment and reveals that in rapidly dividing cells, mRNAs *in vivo* are far less structured than *in vitro*. This scarcity of structure is well suited for the primary role of mRNA as an informational molecule providing a uniform substrate for translating ribosomes. Nonetheless, we identify hundreds of specific mRNA regions that are highly structured *in vivo*, and we show for three examples that these structures affect protein expression. Our studies provide an excellent set of candidate regions, among the truly enormous number of structured regions seen *in vitro*, for exploring the regulatory role of structured mRNAs. The DMS-seq approach is readily extendable to other organisms, including human-derived samples as we show here, and to the analysis of the wide range of functional RNA molecules present in a cell. Thus DMS-seq broadly enables the analysis of structure-function relationships for both informational and functional RNAs. Among the many potential applications, attractive candidates include the analysis of long noncoding RNAs^{25,26}, the relationship between mRNA structure and microRNA/RNA interference targeting²⁷, and functional identification and analysis of ribozymes²⁸, riboswitches²⁹ and thermal sensors³⁰.

METHODS SUMMARY

DMS modification. For *in vivo* DMS modification, 15 ml of exponentially growing yeast (strain BY4741) at 30 °C were incubated with 300–600 µl DMS for 2–4 min (which results in multiple modifications per mRNA molecule). DMS was quenched with the addition of 30 ml stop solution (30% beta-mercaptoethanol (BME), 25% isoamyl alcohol). Total RNA was purified using hot acid phenol (Ambion). PolyA(+) mRNA was obtained using magnetic poly(A)⁺ Dynabeads (Invitrogen).

Library generation. Sequencing libraries were prepared as outlined in Fig. 1. Specifically, DMS-treated mRNA samples were denatured at 95 °C and fragmented in 1× RNA fragmentation buffer (Ambion). Fragments of 60–70 nucleotides were gel-purified and ligated to microRNA cloning linker-1 (IDT) and reverse transcribed

using Superscript III (Invitrogen). Truncated reverse transcription products were gel-purified and circularized using CircLigase (Epicentre). Illumina sequencing adapters were introduced by 8–10 cycles of PCR.

Sequencing and sequence alignment. Raw sequences obtained from Hiseq2000 (Illumina) were aligned against *Saccharomyces cerevisiae* assembly R62 (UCSC: sacCer2). Aligned reads were filtered so that no mismatches were allowed and alignments were required to be unique.

Online resources. For secondary structure models that are supported by DMS-seq and have evidence for phylogenetic conservation, visit <http://weissmanlab.ucsf.edu/yeaststructures/index.html>.

Online Content Any additional Methods, Extended Data display items and Source Data are available in the online version of the paper; references unique to these sections appear only in the online paper.

Received 25 March; accepted 25 November 2013.

Published online 15 December 2013.

1. Gruber, A. R., Neuböck, R., Hofacker, I. L. & Washietl, S. The RNAz web server: prediction of thermodynamically stable and evolutionarily conserved RNA structures. *Nucleic Acids Res.* **35**, W335–W338 (2007).
2. Ouyang, Z., Snyder, M. P. & Chang, H. Y. SeqFold: Genome-scale reconstruction of RNA secondary structure integrating high-throughput sequencing data. *Genome Res.* **23**, 377–387 (2013).
3. Kertesz, M. et al. Genome-wide measurement of RNA secondary structure in yeast. *Nature* **467**, 103–107 (2010).
4. Underwood, J. G. et al. FragSeq: transcriptome-wide RNA structure probing using high-throughput sequencing. *Nature Methods* **7**, 995–1001 (2010).
5. Spitale, R. C. et al. RNA SHAPE analysis in living cells. *Nature Chem. Biol.* **9**, 18–20 (2013).
6. Lucks, J. B. et al. Multiplexed RNA structure characterization with selective 2'-hydroxyl acylation analyzed by primer extension sequencing (SHAPE-Seq). *Proc. Natl Acad. Sci. USA* **108**, 11063–11068 (2011).
7. Deigan, K. E., Li, T. W., Mathews, D. H. & Weeks, K. M. Accurate SHAPE-directed RNA structure determination. *Proc. Natl Acad. Sci. USA* **106**, 97–102 (2009).
8. Wan, Y. et al. Genome-wide measurement of RNA folding energies. *Mol. Cell* **48**, 169–181 (2012).
9. Wells, S. E., Hughes, J. M., Igel, A. H. & Ares, M. Jr. Use of dimethyl sulfate to probe RNA structure *in vivo*. *Methods Enzymol.* **318**, 479–493 (2000).
10. Ben-Shem, A. et al. The structure of the eukaryotic ribosome at 3.0 Å resolution. *Science* **334**, 1524–1529 (2011).
11. Ziehler, W. A. & Engelke, D. R. Probing RNA structure with chemical reagents and enzymes. *Curr. Protoc. Nucleic Acid Chem.* **6**, Unit 6.1 (2001).
12. Zaug, A. J. & Cech, T. R. Analysis of the structure of *Tetrahymena* nuclear RNAs *in vivo*: telomerase RNA, the self-splicing rRNA intron, and U2 snRNA. *RNA* **1**, 363–374 (1995).
13. Cordero, P., Kladwang, W., VanLang, C. C. & Das, R. Quantitative dimethyl sulfate mapping for automated RNA secondary structure inference. *Biochemistry* **51**, 7037–7039 (2012).
14. Inoue, T. & Cech, T. R. Secondary structure of the circular form of the *Tetrahymena* rRNA intervening sequence: a technique for RNA structure analysis using chemical probes and reverse transcriptase. *Proc. Natl Acad. Sci. USA* **82**, 648–652 (1985).
15. Gonzalez, T. N., Sidrauski, C., Dörfler, S. & Walter, P. Mechanism of non-spleosomal mRNA splicing in the unfolded protein response pathway. *EMBO J.* **18**, 3119–3132 (1999).
16. Badis, G., Saveanu, C., Fromont-Racine, M. & Jacquier, A. Targeted mRNA degradation by deadenylation-independent decapping. *Mol. Cel.* **15**, 5–15 (2004).
17. Chartrand, P., Meng, X. H., Singer, R. H. & Long, R. M. Structural elements required for the localization of ASH1 mRNA and of a green fluorescent protein reporter particle *in vivo*. *Curr. Biol.* **9**, 333–338 (1999).
18. Rüegsegger, U., Leber, J. H. & Walter, P. Block of HAC1 mRNA translation by long-range base pairing is released by cytoplasmic splicing upon induction of the unfolded protein response. *Cell* **107**, 103–114 (2001).
19. Zuker, M. Mfold web server for nucleic acid folding and hybridization prediction. *Nucleic Acids Res.* **31**, 3406–3415 (2003).
20. Wittebolle, L. et al. Initial community evenness favours functionality under selective stress. *Nature* **458**, 623–626 (2009).
21. Ingolia, N. T., Ghaemmaghami, S., Newman, J. R. S. & Weissman, J. S. Genome-wide analysis *in vivo* of translation with nucleotide resolution using ribosome profiling. *Science* **324**, 218–223 (2009).
22. Herschlag, D. RNA chaperones and the RNA folding problem. *J. Biol. Chem.* **270**, 20871–20874 (1995).
23. Li, F. et al. Global analysis of RNA secondary structure in two metazoans. *Cell Rep.* **1**, 69–82 (2012).
24. Stade, K. et al. Exportin 1 (Crm1p) is an essential nuclear export factor. *Cell* **90**, 1041–1050 (1997).
25. Kretz, M. et al. Control of somatic tissue differentiation by the long non-coding RNA TINCR. *Nature* **493**, 231–235 (2013).
26. Memczak, S. et al. Circular RNAs are a large class of animal RNAs with regulatory potency. *Nature* (2013).
27. Tan, X. et al. Tiling genomes of pathogenic viruses identifies potent antiviral shRNAs and reveals a role for secondary structure in shRNA efficacy. *Proc. Natl Acad. Sci. USA* **109**, 869–874 (2012).
28. Tang, J. & Breaker, R. R. Structural diversity of self-cleaving ribozymes. *Proc. Natl Acad. Sci. USA* **97**, 5784–5789 (2000).
29. Li, S. & Breaker, R. R. Eukaryotic TPP riboswitch regulation of alternative splicing involving long-distance base pairing. *Nucleic Acids Res.* **41**, 3022–3031 (2013).
30. Meyer, M., Plass, M., Pérez-Valle, J., Eyras, E. & Vilardell, J. Deciphering 3'ss selection in the yeast genome reveals an RNA thermosensor that mediates alternative splicing. *Mol. Cell* **43**, 1033–1039 (2011).

Acknowledgements We thank R. Andino, M. Bassik, J. Doudna, J. Dunn, T. Faust, N. Stern-Ginossar, C. Gross, C. Guthrie, N. Ingolia, C. Jan, M. Kampmann, D. Koller, G.W. Li, S. Mortimer, E. Oh, C. Pop and members of the Weissman laboratory for discussions; J. Stewart-Ornstein and O. Brandman for plasmids; C. Chu, N. Ingolia and J. Lund for sequencing help. This research was supported by the Center for RNA Systems Biology (J.S.W.), the Howard Hughes Medical Institute (J.S.W.), and the National Science Foundation (M.Z.).

Author Contributions S.R., M.Z. and J.S.W. designed the experiments. S.R. and M.Z. performed the experiments, and S.R. analysed the data. S.W. and M.K. completed the phylogenetic analysis. S.R., M.Z. and J.S.W. drafted and revised the manuscript.

Author Information All data are deposited in Gene Expression Omnibus (accession number GSE45803). Reprints and permissions information is available at www.nature.com/reprints. The authors declare no competing financial interests. Readers are welcome to comment on the online version of the paper. Correspondence and requests for materials should be addressed to J.S.W. (weissman@cmp.ucsf.edu).

METHODS

Media and growth conditions. Yeast strain BY4741 was grown in YPD at 30 °C. Saturated cultures were diluted to $D_{600\text{nm}}$ of approximately 0.09 and grown to a final $D_{600\text{nm}}$ of 0.7 to 0.8 in YPD at the time of DMS treatment or mRNA collection. For ATP depletion experiments, cells were incubated for 1 h in 10 mM sodium azide and 10 mM deoxyglucose before DMS treatment³¹. For 10 °C experiments, cells were grown to exponential phase and shifted to 10 °C by diluting the 30 °C media with 4 °C media. Mammalian cells were grown and treated with DMS in log phase (K562 cells) or at ~80% confluency for adherent cells (human foreskin fibroblasts).

DMS modification. For *in vivo* DMS modification, 15 ml of exponentially growing yeast at 30 °C were incubated with 300–600 µl DMS for 2–4 min (which results in multiple modifications per mRNA molecule). Cells at 10 °C were incubated with 400 µl DMS for 40 min to achieve similar modification levels as cells grown at 30 °C. DMS was quenched by adding 30 ml stop solution (30% β-mercaptoethanol, 25% isoamyl alcohol) after which cells were quickly put on ice, collected by centrifugation at 3,000g and 4 °C for 3 min, and washed with 15 ml 30% BME solution. Cells were then resuspended in total RNA lysis buffer (10 mM EDTA, 50 mM sodium acetate pH 5.5), and total RNA was purified with hot acid phenol (Ambion). PolyA(+) mRNA was obtained using magnetic poly(A)⁺ Dynabeads (Invitrogen). For *in vitro* and denatured DMS modifications, mRNA was collected in the same way as described above but from yeast that were not treated with DMS or quench solution. 4 µg of mRNA was denatured at 95 °C for 2 min and either incubated in 0.2% DMS for 1 min (denatured control sample) or cooled on ice and refolded in RNA folding buffer (10 mM Tris pH 8.0, 100 mM NaCl, 6 mM MgCl₂) at 30 °C for 30 min then incubated in 3–5% DMS for 2–5 min (*in vitro* sample). For intact ribosomes, polysomes were isolated on a sucrose gradient and treated with 4% DMS at 10 °C for 40 min in polysome gradient buffer (20 mM Tris pH 8.0, 150 mM KCl, 0.5 mM dithiothreitol (DTT), 5 mM MgCl₂). DMS amounts/times were chosen to give a similar overall level of modification for the *in vivo*, *in vitro* and denatured sample. For *in vitro* probing at different temperatures, the RNA was refolded at 45 °C, 60 °C, or 70 °C. The DMS was quenched using 30% BME, 0.3 M sodium acetate pH 5.5, 2 µl GlycoBlue solution and precipitated with 1× volume of 100% isopropanol. For K562 cells, 15 ml of cells were treated with 300 µl (*in vivo* replicate 1) or 400 µl (*in vivo* replicate 2) DMS and modified for 4 min. DMS was quenched by adding 30 ml of 30% BME solution after which cells were quickly put on ice, collected by centrifugation at 1,000g at 4 °C for 3 min, and washed twice with 15 ml 30% BME solution. For fibroblast cells, 15 cm² plates with 15 ml of media were treated with 300 µl DMS for 4 min. The DMS was decanted and the plates were washed twice in 30% BME stop solution. Both K562 cells and fibroblasts were resuspended in TRIzol Reagent and total RNA was isolated. PolyA(+) mRNA was obtained using Oligotex resin (Qiagen).

Library generation. Sequencing libraries were prepared as outlined in Fig. 1 with a modified version of the protocol used for ribosome profiling³². Specifically, DMS treated mRNA samples were denatured for 2 min at 95 °C and fragmented at 95 °C for 2 min in 1× RNA fragmentation buffer (Zn²⁺ based, Ambion). The reaction was stopped by adding 1/10 volume of 10× Stop solution (Ambion) and quickly placed on ice. The fragmented RNA was run on a 10% TBU (Tris borate urea) gel for 60 min. Fragments of 60–70 nucleotides in size were visualized by blue light (Invitrogen) and excised. Gel extraction was performed by crushing the purified gel piece and incubating in 300 µl DEPC-treated water at 70 °C for 10 min with vigorous shaking. The RNA was then precipitated by adding 33 µl sodium acetate, 2 µl GlycoBlue (Invitrogen), and 900 µl 100% ethanol, incubating on dry ice for 20 min and spinning for 30 min at 4 °C. The samples were then resuspended in 7 µl 1× PNK buffer (NEB) and the 3' phosphates left after random fragmentation were resolved by adding 2 µl T4 PNK (NEB), 1 µl of SUPERase Inhibitor (Ambion) and incubating at 37 °C for 1 h. The samples were then directly ligated to 1 µg of microRNA cloning linker-1, /5rApp/CTGTAGGCACCATCAAT/3ddC/ (IDT DNA) by adding 2 µl T4 RNA ligase2, truncated K227Q (NEB), 1 µl 0.1 M DTT, 6 µl 50% PEG, 1 µl 10× ligase2 buffer, and incubating at room temperature for 1.5 h. Ligated products were run on a 10% TBU gel for 40 min, visualized by blue light, and separated from unligated excess linker-1 by gel extraction as described above. Reverse transcription was performed in 20 µl volume at 52 °C using Superscript III (Invitrogen), and truncated reverse transcription products of 25–45 nucleotides (above the size of the reverse transcription primer) were extracted by gel purification. The samples were then circularized using CircLigase (Epicentre), and Illumina sequencing adaptors were introduced by 8–10 cycles of PCR.

Sequencing and sequence alignment. Raw sequences obtained from Hiseq2000 (Illumina) corresponding to the DNA sequence from the reverse transcription termination products were aligned as described³³, against *Saccharomyces cerevisiae* assembly R62 (UCSC: sacCer2) downloaded from the *Saccharomyces* Genome Database on October 11, 2009 (SGD, <http://www.yeastgenome.org/>). Aligned reads were filtered so that no mismatches were allowed and alignments were required to

be unique. Mammalian cells data was aligned to a transcript collection downloaded from RefSeq (<http://www.ncbi.nlm.nih.gov/refseq/>), in which each gene is represented by its longest protein-coding transcript. Aligned reads were filtered so that no more than 2 mismatches were allowed and the alignments were required to be unique. All data are deposited in Gene Expression Omnibus (accession number GSE45803).

Computing the DMS signal. For the ribosomal RNA, the raw data were normalized proportionally to the most highly reactive residue after removing the outliers by 90% Winsorization (all data above the 95th percentile is set to the 95th percentile)³⁴. For the mRNA, the raw data was normalized proportionally to the most highly reactive base within the given structured window. Normalization of DMS data in windows of 50–200 nucleotides counteracts artefacts caused by mRNA fragmentation before polyA selection, which can lead to increased overall signal towards the 3' end of longer messages (as any 5' end that was broken off before the polyA(+)) selection would be lost after the polyA(+) selection).

Computing the agreement with ribosomal RNA. The secondary structure models for yeast ribosomal RNAs were downloaded from Comparative RNA Website and Project database (<http://www.rna.icmb.utexas.edu/DAT/3C/Structure/index.php>). The crystal structure model was downloaded from Protein Data Bank (<http://www.pdb.org/pdb/search/structidSearch.do?structureId=3u5b>). The solvent-accessible surface area³⁵ was calculated in PyMOL, and DMS was modelled as a sphere with 3 Å radius (representing a conservative estimate for accessibility because DMS is a flat molecule). Accessible residues were defined as residues with solvent accessibility area of greater than 2 Å². True positive bases were defined as bases that are both unpaired in the secondary structure model and solvent-accessible in the crystal structure model. True negative bases were defined as bases that are paired (A-U or C-G specifically) in the secondary structure model. The DMS data was normalized as described above. Accuracy was calculated as the number of true positive bases plus the number of true negative bases divided by all tested bases.

Secondary structure models. Secondary structure models were generated using mfold³⁶. Colour coding by DMS signal was done using VARNA (<http://varna.lri.fr/>).

In vivo and in vitro DMS analysis. *Saccharomyces cerevisiae* transcriptome coordinates were taken from ref. 37. In total we collected between 140 million and 200 million reads that uniquely aligned to the yeast genome per each sample (*in vivo*, *in vitro* and denatured). Raw data was filtered for messages that have at least 15 reads on average per A or C position. The full yeast data set is comprised of two biological and two technical *in vivo* replicates, two biological and one technical *in vitro* replicates, and two biological and one technical denatured replicates. For mammalian K562 data set we collected two biological *in vivo* replicates (at 2% DMS and 2.7% DMS), one *in vitro*, and one denatured samples. For mammalian fibroblast data we collected of one *in vivo*, one *in vitro*, and one denatured samples. Sliding non-overlapping windows spanning a specified number of As and Cs starting at the 5' UTR were used to parse each message into a number of regions. Regions with matching length were taken from the 18S ribosomal RNA. A Gini index and r value relative to that of a denatured control was calculated for each region. Highly structured regions in windows of 50 A or C nucleotides were defined with r value < 0.55 and Gini index > 0.14 to encompass the *in vivo* regions containing validated structures and ribosomal RNA. Regions that are denatured *in vivo* were defined with r value > 0.70 and Gini index < 0.08. Melting temperature (T_{melt}) was defined as the lowest temperature where the DMS signal for a given mRNA region resembles denatured and was estimated based on the temperature at which a region reached r ≥ 0.70 or Gini index ≤ 0.11. This represents relaxed criteria for unfolding to avoid bias towards overestimating thermostability of regions due to sample variability caused by sequencing depth of *in vitro* temperature samples (which have five to tenfold less coverage than the *in vivo*, *in vitro* (30 °C) and denatured samples). For metagene analyses, the DMS signal was normalized in windows of 200 A or C nucleotides (relative to the top five most reactive residues), and the *in vivo* data was normalized by the denatured. Translation efficiency (TE) per message was calculated as number of ribosome footprints divided by the number of mRNA fragments.

Conservation analysis. For a list of regions as well as secondary structure models supported by DMS data and conservation analysis visit <http://weissmanlab.ucsf.edu/yeaststructures/index.html>.

Multiple sequence alignments generated by MultiZ³⁸ were downloaded from <http://hgdownload.cse.ucsc.edu/goldenPath/sacCer2/multiz7way>. Small (50 As or Cs) and large (100 As or Cs) overlapping regions with evidence for structure from the DMS probing experiment were inspected by the phylogenetic conservation analysis. The consensus secondary structure prediction was compared to normalized DMS data. The DMS values were separated in two groups for paired and unpaired bases, respectively. The median of both groups and the P value from a one-sided Wilcoxon rank sum test is reported, testing the hypothesis that unpaired bases have higher DMS values. Both distributions are shown as box plots for each region on the website. For each region (1) a consensus secondary structure was predicted

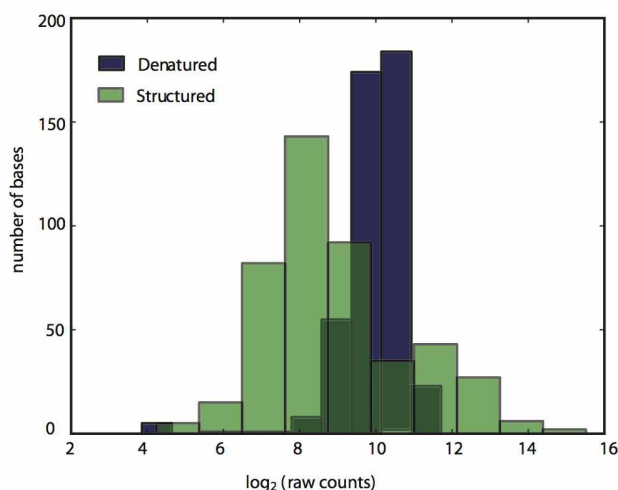
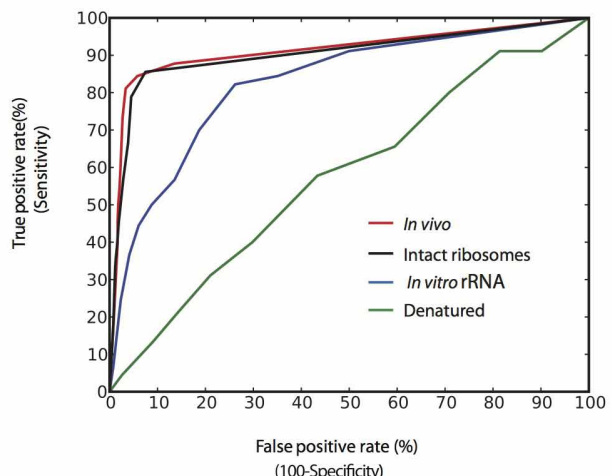
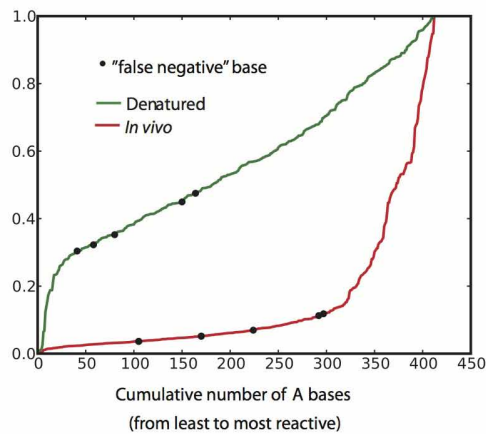
and (2) the consensus structure was assessed for features typical of a functional RNA. The consensus secondary structure (1) was done using RNAalifold³⁹, which extends the classical thermodynamic folding for single sequences in two ways: it averages over the sequences while evaluating the energy for a given fold and it adds “pseudoenergies” to account for consistent or inconsistent mutations. The goal is to find the structure of the minimum free energy in this extended energy model. RNAalifold readily predicts a consensus structure even if there is no selection pressure for a conserved RNA structure. RNAz^{40,41} was used to address the question if a predicted structure is likely to be a functional structure that is evolutionarily conserved. RNAz calculates two metrics typical for functional RNAs: thermodynamic stability and evolutionary conservation. RNAz calculates a z-score indicating how much more stable a structure is compared to a random background of sequences of the same dinucleotide content. By convention, negative z-score indicates more stable structures and all reported z-scores are the average of all sequences in the alignment. RNAz calculates a metric known as structure conservation index (SCI). The SCI takes values between 0 and 1.0, 0 means there is no structure conserved at all, 1 means the structure is perfectly conserved. The SCI is not normalized with respect to sequences conservation, so an alignment with sequences 100% conserved has by definition SCI = 1.0. RNAz evaluates z-score, SCI and sequence diversity of the alignment and provides an overall classification score that is based on a support vector machine classifier. It ranges from very negative values with little evidence for a functional RNA, over 0 which means undecided to high positive values with good evidence for a functional RNA. For convenience, this score is mapped to a probability of being a functional RNA which is reported in the results (the higher the better). A total of 189 structures with RNAz significance value >0.5 and a correlation P value between the predicted structure and the DMS signal of <0.01 are displayed on the aforementioned website.

Functional UTR cloning. A fluorescent Venus reporter driven by a Nop8 promoter (chromosome XV:52262–53096) and *C. albicans* *ADH1* terminator was genetically integrated into yeast strain BY4741 at the *TRP1* locus (chromosome IV:461320–462280). Plasmids containing kanamycin resistance and the untranslated region (UTR) of interest were made in a pUC18 plasmid backbone (Thermo Scientific). For the *PMA1* 5' UTR, the entire 1-kb promoter region and 5' UTR (chromosome VII:482672–483671) was used. The pNop8 promoter was retained for the *SFT2* 5' UTR investigation, with only the Nop8 5' UTR replaced by the *SFT2* 5' UTR. All 3' UTRs were cloned to include > 100 base pairs after evidence of transcription ends (see Extended Data Figs 5 and 6 and Extended Data Table 1 for sequence of *PMA1*, *SFT2* and *PRC1* structures). BY4741-Venus yeast were

transformed using the standard technique of homologous recombination from a plasmid PCR product containing either a wild-type, mutant or compensated UTR. Successfully transformed yeast were identified by check PCR and subsequently sequenced to confirm the presence of only the desired mutations.

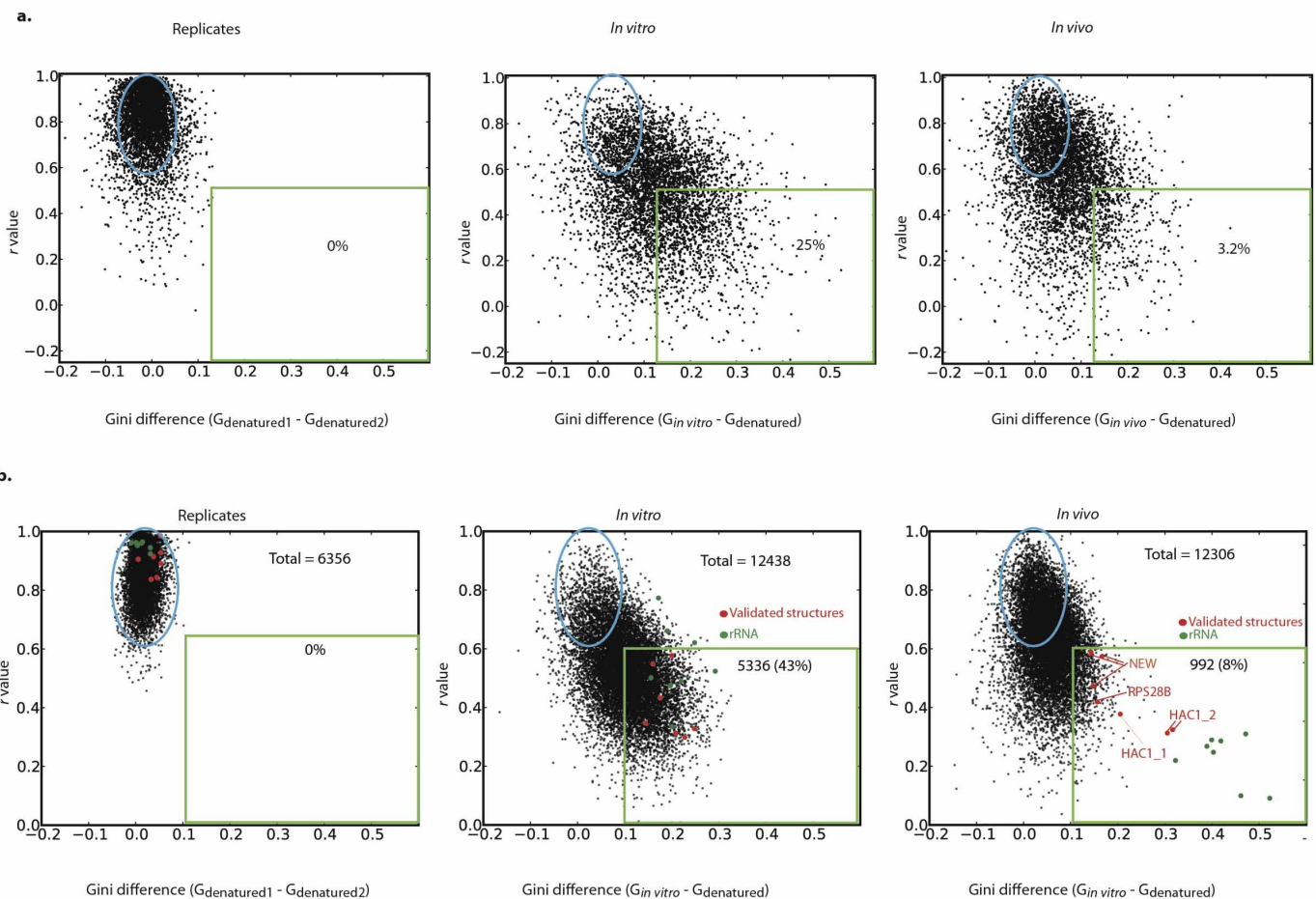
Flow cytometry. A saturated yeast culture was diluted 1:200 fold in minimal media and grown at 30 °C for 6–8 h before flow cytometry using a LSRII flow cytometer (Becton Dickinson) and 530/30 filter. 10 °C cultures were grown for 72 h. Venus signal from each cell was normalized to cell size (Venus/side scatter) using Matlab 7.8.0 (Mathworks)⁴², and once normalized, all events (~20,000 per experiment) were averaged for a final Venus/side scatter value.

31. Kortmann, J., Sczodrok, S., Rinnenthal, J., Schwalbe, H. & Narberhaus, F. Translation on demand by a simple RNA-based thermosensor. *Nucleic Acids Res.* **39**, 2855–2868 (2011).
32. Ingolia, N. T., Brar, G. A., Rouskin, S., McGeechey, A. M. & Weissman, J. S. The ribosome profiling strategy for monitoring translation *in vivo* by deep sequencing of ribosome-protected mRNA fragments. *Nature Protocols* **7**, 1534–1550 (2012).
33. Ingolia, N. T., Ghaemmaghami, S., Newman, J. R. S. & Weissman, J. S. Genome-wide analysis *in vivo* of translation with nucleotide resolution using ribosome profiling. *Science* **324**, 218–223 (2009).
34. Hastings, C., Mosteller, F., Tukey, J. W. & Winsor, C. P. Low moments for small samples: a comparative study of order statistics. *Ann. Math. Stat.* **18**, 413–426 (1947).
35. Lee, B. & Richards, F. M. The interpretation of protein structures: estimation of static accessibility. *J. Mol. Biol.* **55**, 379–400 IN3–IN4 (1971).
36. Zuker, M. Mfold web server for nucleic acid folding and hybridization prediction. *Nucleic Acids Res.* **31**, 3406–3415 (2003).
37. Nagalakshmi, U. *et al.* The transcriptional landscape of the yeast genome defined by RNA sequencing. *Science* **320**, 1344–1349 (2008).
38. Blanchette, M. *et al.* Aligning multiple genomic sequences with the threaded blockset aligner. *Genome Res.* **14**, 708–715 (2004).
39. Bernhart, S. H., Hofacker, I. L., Will, S., Gruber, A. R. & Stadler, P. F. RNAalifold: improved consensus structure prediction for RNA alignments. *BMC Bioinformatics* **9**, 474 (2008).
40. Washietl, S., Hofacker, I. L. & Stadler, P. F. Fast and reliable prediction of noncoding RNAs. *Proc. Natl Acad. Sci. USA* **102**, 2454–2459 (2005).
41. Gruber, A. R., Findeiß, S., Washietl, S., Hofacker, I. L. & Stadler, P. F. Rnaz 2.0: improved noncoding RNA detection. *Pac. Symp. Biocomput.* 69–79 (2010).
42. Brandman, O. *et al.* A ribosome-bound quality control complex triggers degradation of nascent peptides and signals translation stress. *Cell* **151**, 1042–1054 (2012).

a**b****c**

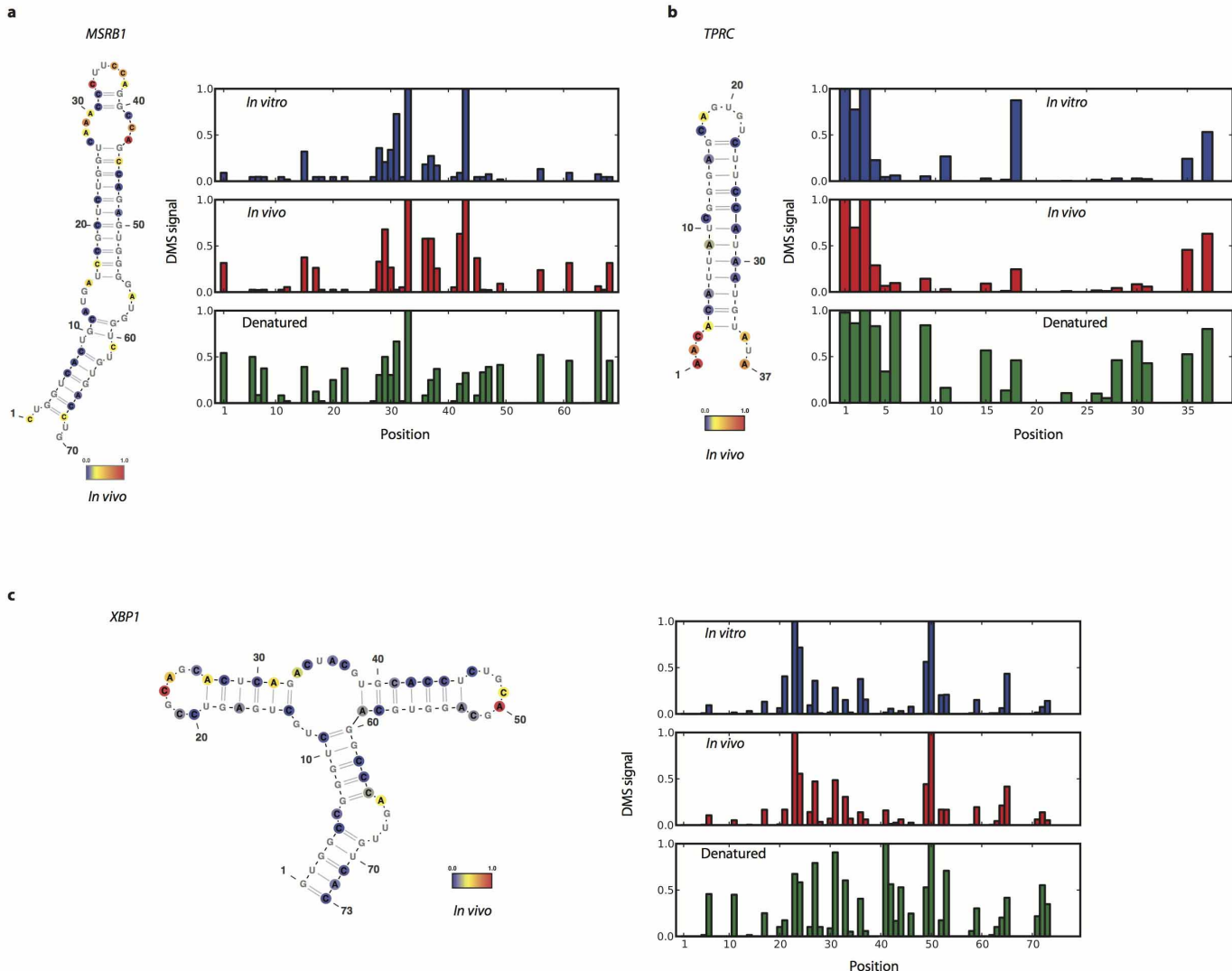
Extended Data Figure 1 | Ribosomal RNA analysis. **a**, Histogram of raw counts distribution for denatured and structured 18S rRNA. $\log_2(\text{raw counts})$ for A bases plotted for *in vivo* and denatured samples. **b**, ROC curve on the DMS signal for A and C bases from the 25S rRNA in denatured, *in vitro*, intact ribosomes, and *in vivo* samples. True positives are defined as bases that are both

unpaired and solvent-accessible, and true negatives are defined as bases that are paired. **c**, DMS signal on all of the 18S rRNA A bases plotted from least to most reactive in the denatured or *in vivo* samples. The A bases that are false negatives relative to the crystal structure are coloured as black dots on both the denatured and *in vivo* samples.



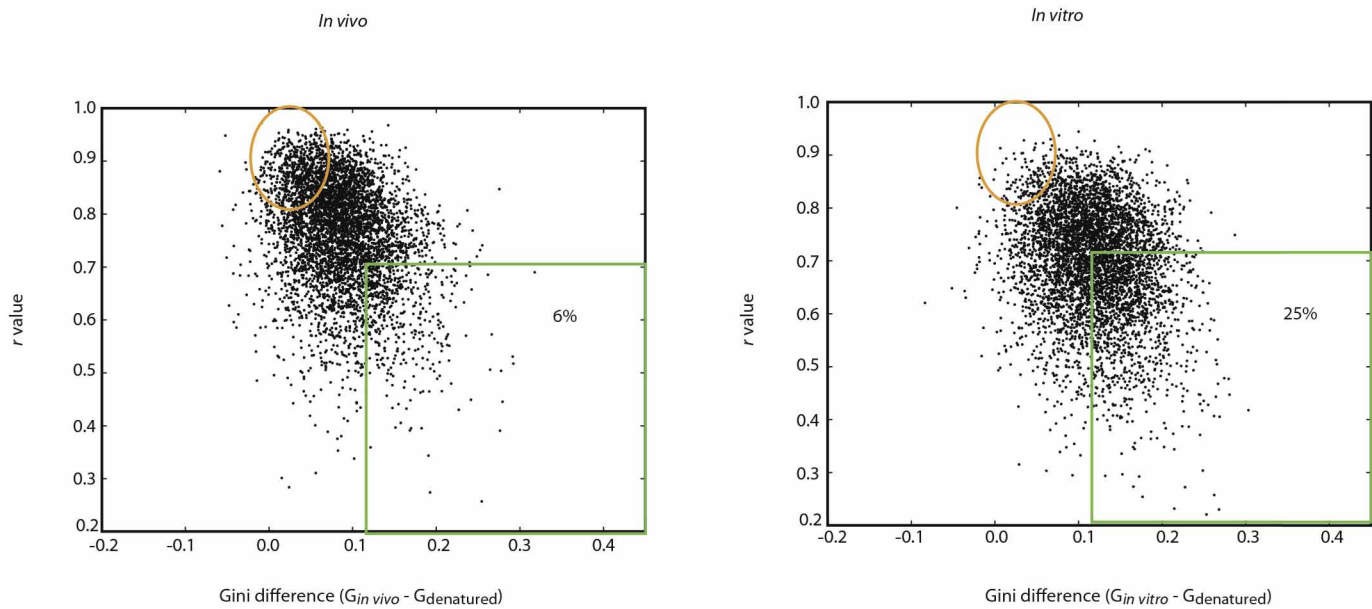
Extended Data Figure 2 | mRNA structure analysis with different window sizes. **a, b**, Scatter plots of Gini index versus r values in replicate samples and for *in vivo* or *in vitro* samples relative to denatured sample for mRNA regions with an average of at least 15 counts per position, spanning the sequence of

25 A/C nucleotides (5,000 randomly selected regions are shown) (a) or 100A/C nucleotides (b). Shown are regions spanning validated secondary structures (red dots) and regions from the 18S rRNA (green dots).



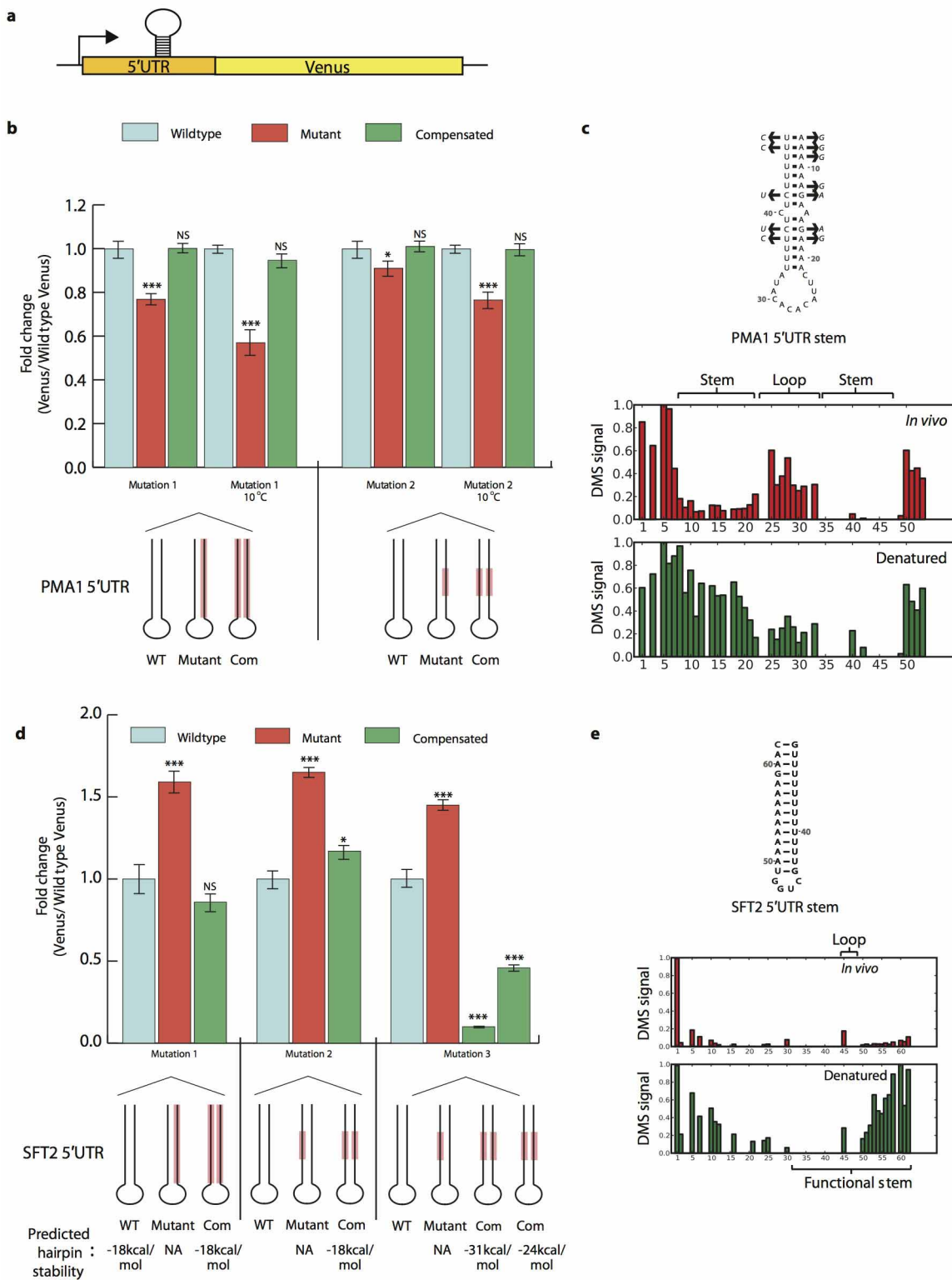
Extended Data Figure 3 | Agreement of DMS-seq with validated structures in mammalian K562 cells. Raw DMS counts were normalized to the most reactive nucleotide in the given region. A and C bases were normalized separately. **a**, The DMS signal is colour coded proportional to intensity and plotted onto the secondary structure model of *MSRB1* selenocysteine insertion

element, nucleotide 1 corresponds to nucleotide 966 of the transcript. **b**, *TPRC* iron recognition element, nucleotide 1 corresponds to nucleotide 3901 of the transcript. **c**, *XBP1* conserved non canonical intron recognized by Ire1, nucleotide 1 corresponds to nucleotide 520 of the transcript.



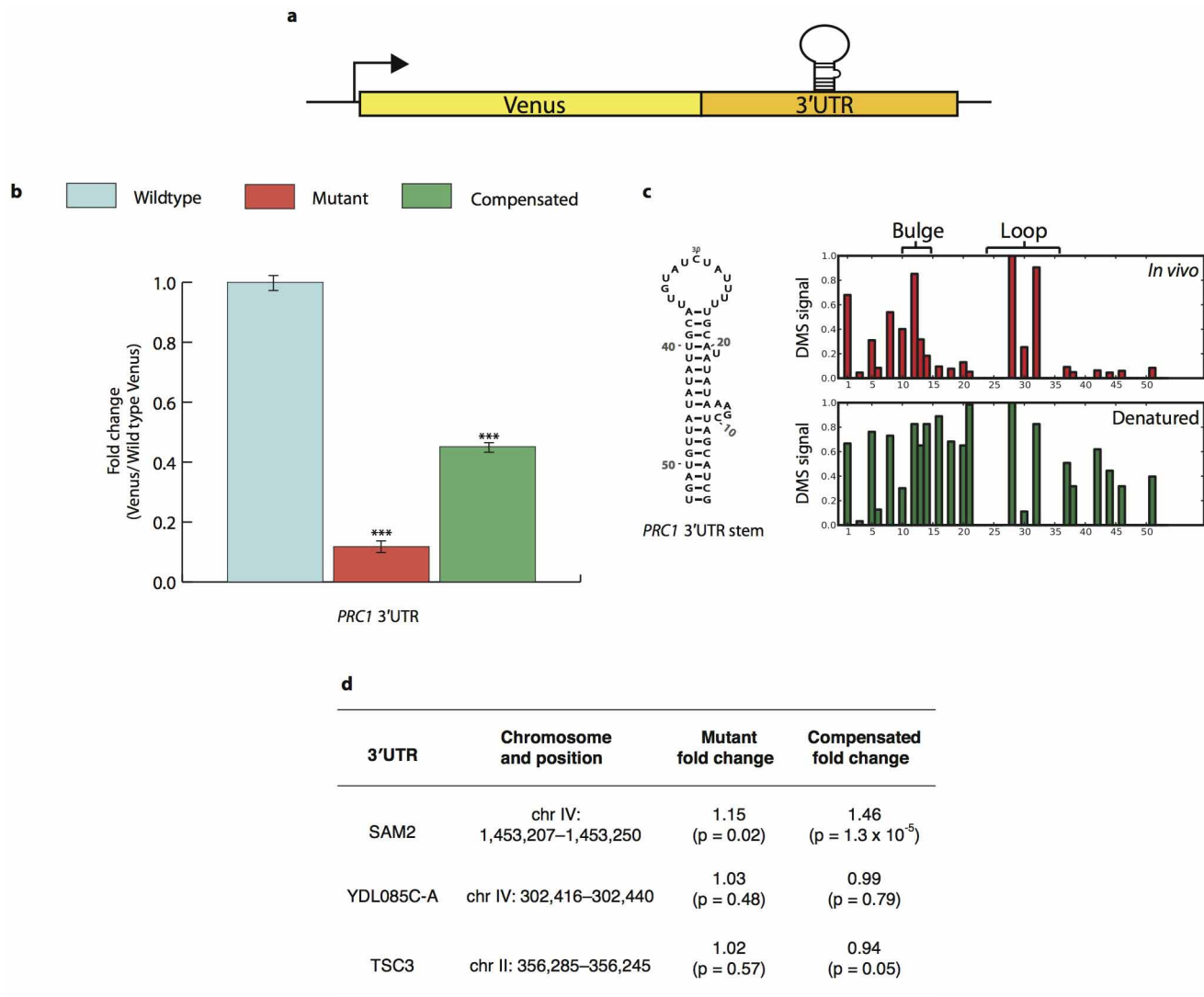
Extended Data Figure 4 | Global mRNA analysis of human foreskin fibroblast cells. Scatter plots of Gini index versus r values for *in vivo* or *in vitro*

samples relative to denatured sample for mRNA regions spanning the sequence of 50 A/C nucleotides.



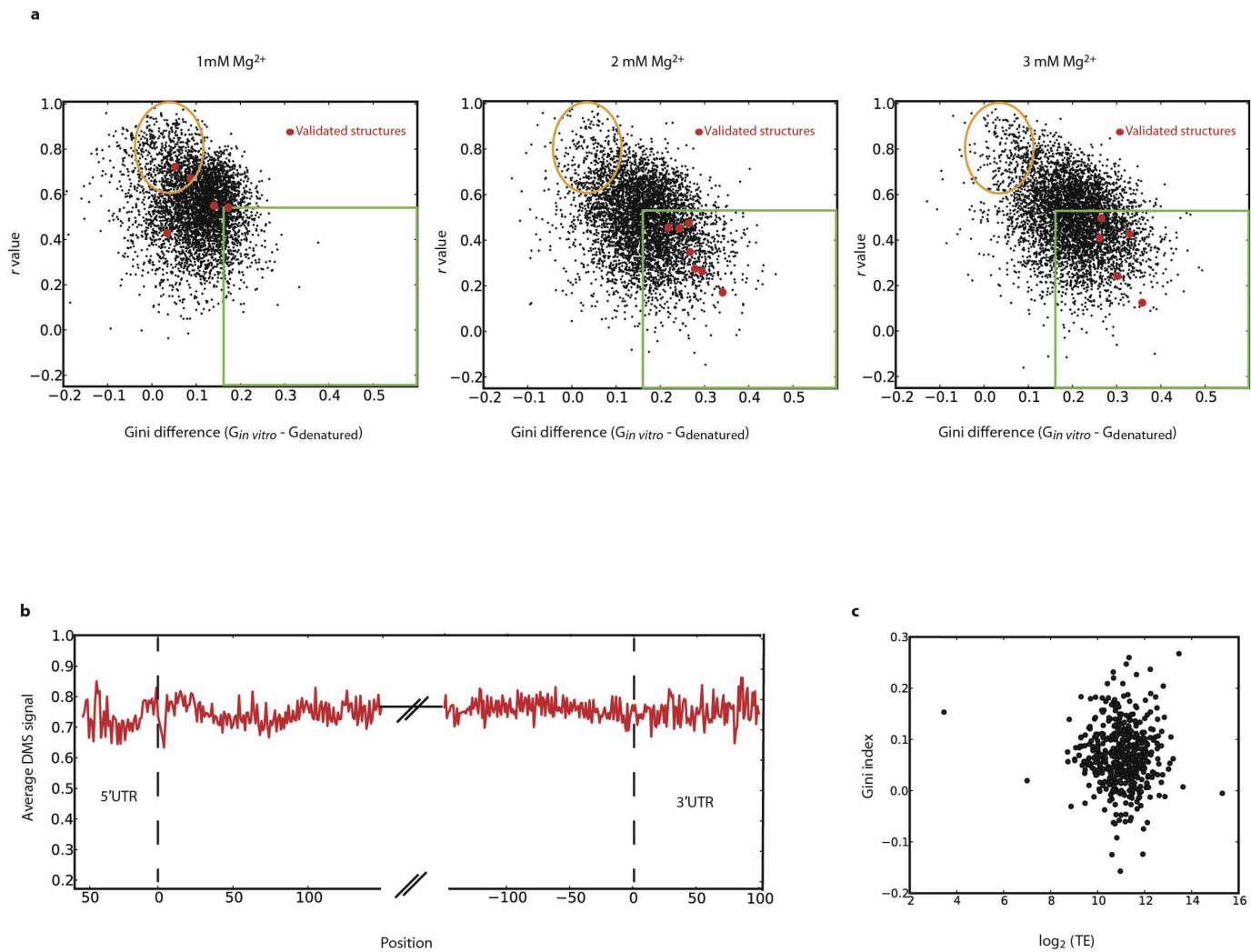
Extended Data Figure 5 | Functional verification of novel 5' UTR structures *in vivo*. **a**, Putative 5' UTR stems were manipulated in the context of a Venus reporter *in vivo*. **b**, PMA1 5' UTR structure was mutated and compensated twice with Venus reporter, differing in number and character of bases mutated. Mutation location shown in red on schematic. Reported *P* values relative to wild-type Venus levels, calculated by two-sided *t*-test (**P* < 0.01, ***P* < 0.001, ****P* < 0.0001). For all graphs, Venus signal normalized to cell size before calculating fold change and data presented is from two biological and two technical replicates. Error bars represent s.e.m. **c**, Secondary structure of functional PMA1 5' UTR stem, with compensatory mutations (arrows)

found in *Saccharomyces paradoxus*, *Saccharomyces mikatae*, *Saccharomyces kudriavzevii* and *Saccharomyces bayanus*. Raw DMS signal shown below (position 1 = chromosome VII:482745). **d**, SFT2 5' UTR structure was mutated and compensated three times in Venus reporter system, differing in number, character and location of bases mutated. Mutation location shown in red on schematic. Stem stability as predicted by mfold. Reported *P* values relative to wild-type Venus levels, also by two-sided *t*-test (**P* < 0.01, ***P* < 0.001, ****P* < 0.0001). Error bars represent standard deviation. **e**, Secondary structure of functional SFT2 5' UTR stem. Position 1 = chromosome II:24023.



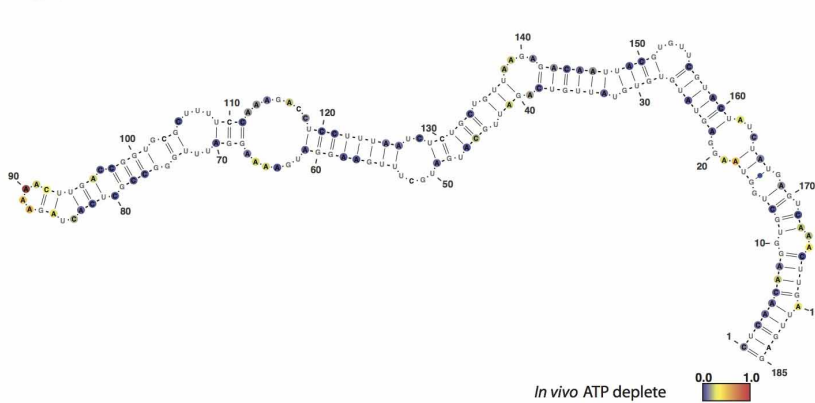
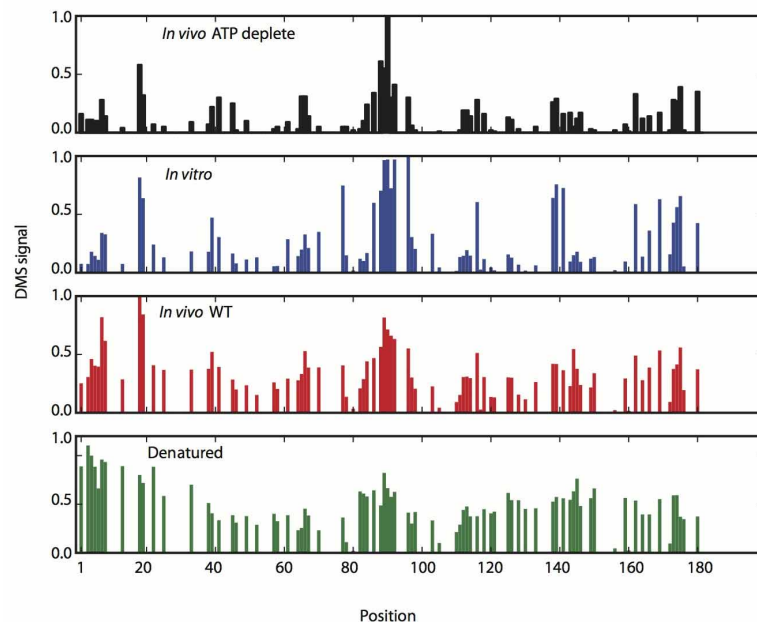
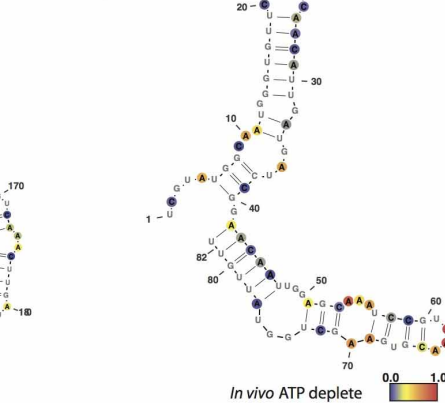
Extended Data Figure 6 | Functional verification of novel *PRC1* 3' UTR structure *in vivo*. **a**, Putative 3' UTR stems were manipulated in the context of a Venus reporter *in vivo*, followed by Venus quantification with flow cytometry. **b**, *PRC1* 3' UTR structure was mutated and compensated in Venus reporter system. For all data, reported *P* values relative to wild-type Venus levels, calculated by two-sided *t*-test (**P* < 0.01, ***P* < 0.001, ****P* < 0.0001). Venus signal was normalized to cell size with fold change reported relative to Venus

levels seen with the wild-type stem. All results shown are derived from four measurements: two biological and two technical replicates. Error bars show standard deviation. **c**, Secondary structure of functional *PRC1* 3' UTR stem, shown with raw DMS signal for *in vivo* and denatured samples. Position 1 = chromosome XIII:863554. **d**, Weakly structured 3' UTRs *in vivo* were tested for function as in **b**, but reveal little effect when mutated and no evidence for compensation.

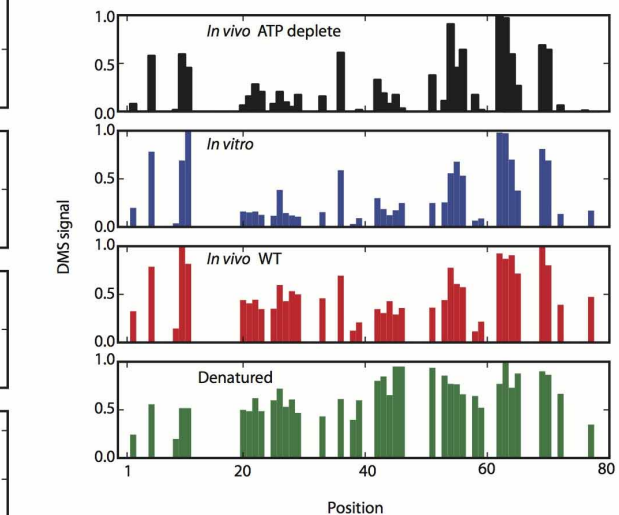


Extended Data Figure 7 | Global analysis of mRNA structure. **a**, *In vitro* DMS-seq on RNA refolded in different Mg^{2+} concentrations. **b**, Metagene plot of the average DMS signal (normalized to denatured control) over 5' UTR,

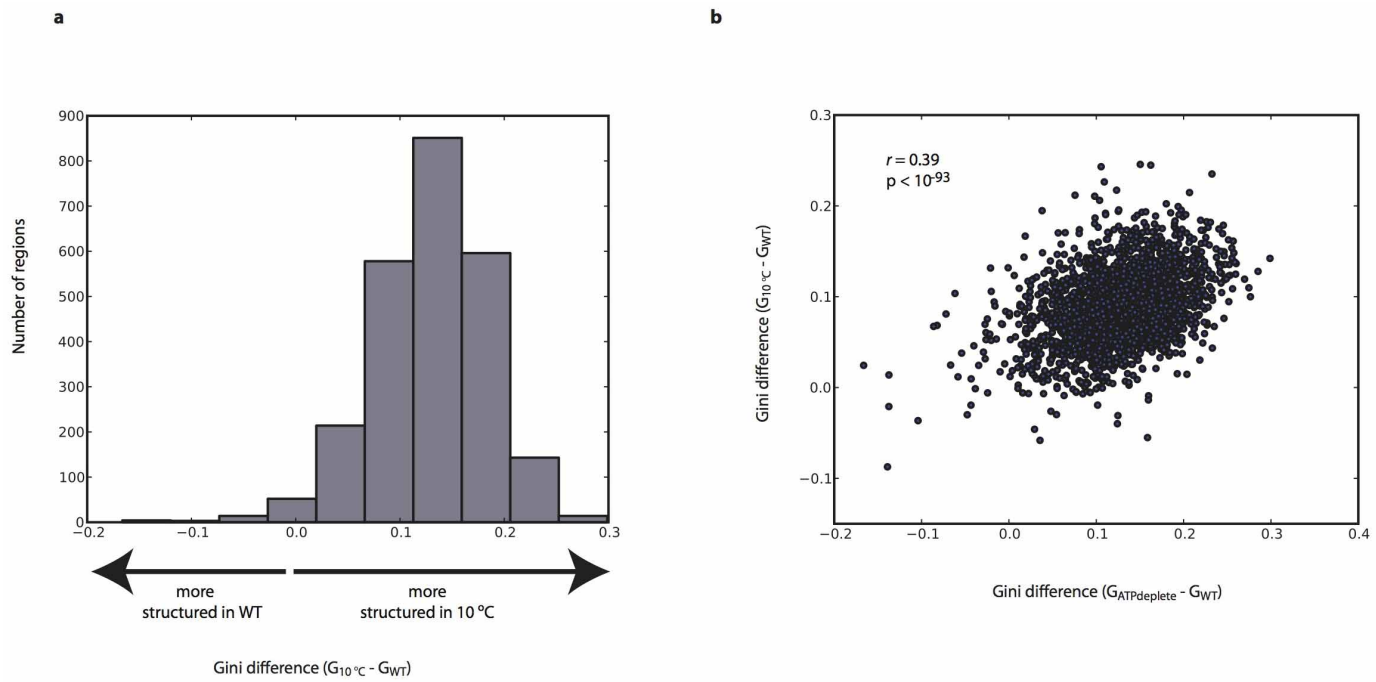
coding, and 3' UTR regions. **c**, Scatter plot of Gini index (calculated over the first 100 A/C bases) of *in vivo* messages (relative to denatured) versus translation efficiency.

a CBF5**b TCP1**

Extended Data Figure 8 | *In vivo* structures forming in ATP depleted conditions. **a, b,** Raw DMS counts were normalized to the most reactive nucleotide in a given region. **a,** The DMS signal is colour coded proportional



to intensity and plotted onto the mfold predicted secondary structure model of CBF5, nucleotide 1 corresponds to chromosome XII position 506479. **b,** TCP1, nucleotide 1 corresponds to chromosome IV position 887991.



Extended Data Figure 9 | Analysis of mRNA structure at 10°C .
a, Histogram of Gini index difference (calculated over 100A or Cs) between 10°C and wild-type (30°C) samples. **b**, Scatter plot of the Gini index

differences in ATP depleted or 10°C yeast relative to wild-type yeast calculated over 50 As or Cs.

Extended Data Table 1 | Sequences of functional structure mutations

UTR	Stem Sequence (5' to 3')
PMA1 Wildtype	TTTTTCTcTCTTTatacacacattcAAAAGAaAGAAAAAA
PMA1 Mutant 1	TTTTTCTcTCTTTatacacacattc <u>TTTCTcTCTTTTT</u>
PMA1 Compensated 1	<u>AAAAAAGAaAGAAA</u> atacacacattc <u>TTTCTcTCTTTTT</u>
PMA1 Mutant 2	TTTTTCTcTCTTTatacacacattc <u>AAATTCATTAAAAA</u>
PMA1 Compensated 2	TTTTAAGCGAGTTatacacacattc <u>AAATTCATTAAAAA</u>
SFT2 Wildtype	GTTTTTTTTTGctggTAAAAAAAAGAAC
SFT2 Mutant 1	<u>CAAAAAAAAAAA</u> TctggTAAAAAAAAGAAC
SFT2 Compensated 1	<u>CAAAAAAAAAAA</u> TctggGTTTTTTTTTG
SFT2 Mutant 2	GTTTTTTTTTGctgg <u>TAAATTTT</u> GAAC
SFT2 Compensated 2	GTTT <u>AAAAAATTT</u> Gctgg <u>TAAATTTT</u> GAAC
SFT2 Mutant 3	GTTTTTTTTTGctggTAA <u>ACCCCCCGAAC</u>
SFT2 Compensated 3	GTTT <u>GGGGGTTT</u> GctggTAA <u>ACCCCCCGAAC</u>
PRC1 Wildtype	GCTACGATcgaaATATA <u>tACGTtttatctatgttACGTTATATATTGTAGT</u>
PRC1 Mutant	<u>TGATGTTAcgaaTATATtTGCA</u> tttatctatgttACGTTATATATTGTAGT
PRC1 Compensated	<u>TGATGTTAcgaaTATATtTGCA</u> tttatctatgtt <u>TGCAATATATAGCATCG</u>

5'-3' mRNA structure sequences are listed. Lowercase letters correspond to non-paired bases, found in bulges or loops within the stem. Mutated bases are underlined.